Life-Cycle Cost Optimization of Wind-excited Tall Buildings using Surrogate Models

Laura Micheli[1], Alice Alipour[2], Simon Laflamme[3]
[1]Assistant Professor, Department of Civil and Environmental Engineering,
Catholic University of America
Corresponding author: michelil@cua.edu
[2]Associate Professor, Department of Civil, Construction and Environmental Engineering,
Iowa State University
[3]Associate Professor, Department of Civil, Construction and Environmental Engineering,
Iowa State University

Abstract

As buildings become taller and slender, they become more sensitive to wind-induced vibrations. Commonly used solutions to mitigate wind-induced vibrations are structural system modifications and integration of supplemental damping devices. This paper presents a procedure to optimize the structural system and the damping device configuration with the goal of reducing wind-induced vibrations. The performance of the building is expressed in terms of life-cycle cost (LCC), allowing to consider not only the initial costs associated with the integration of wind-induced vibration mitigation system but also the lifetime savings due to vibrations suppression. The proposed procedure employs a set of Kriging surrogate models to analyze a large number of different structural properties-damping device characteristics. The combination that minimizes the LCC is taken as the optimal configuration. The procedure is demonstrated on a wind-sensitive 39-story building equipped with passive dampers. Results demonstrated that the accuracy of the Kriging surrogate models depends on the number of input variables considered, with an average root mean square error of 2.5% for the floors without dampers and 5% for the floors equipped with damping devices, respectively. It was also demonstrated that optimal stiffness-damping device configuration and LCC depend on the assumed cost of the structural system modifications.

Keywords: surrogate model, Kriging, tall buildings, life-cycle cost, damping devices, optimization, vibration mitigation, wind mitigation

1. Introduction

Recent advances in construction techniques and modern high-performance materials enabled engineers to design tall buildings of ever-growing heights. As buildings become taller, they become more sensitive to wind-induced vibrations due to their increased flexibility. While the resistance to static wind loads can be attained through a traditional structural system appropriately designed following code-specified standards (i.e., ASCE 7-16 [1]), serviceability and habitability are yet major challenges. Also, excessive wind-induced vibrations ignored through the static approach could produce undesired effects, including building occupants' discomfort, damage to nonstructural elements, and in some cases sudden failures of structural components. As a result, various solutions have been proposed to reduce wind-induced vibrations in tall buildings [48]. These solutions can be broadly classified as: aerodynamic shape modification, modification of the structural system, and integration of supplemental energy dissipation devices [2, 3]. The first

solution consists of modifying the external shape of the building and its cross-section to improve the aerodynamic and aeroelasticity of the structure, with consequent reduction of wind load effects [4, 5]. The second solution is the most common choice for structural designers and it consists of modifying the structural system, for example increasing the stiffness of the building, to reach serviceability performance targets [6, 7, 8]. The third solution is the integration of motion control devices in the structural system, including passive, semi-active, active, and hybrid control devices [9, 10, 11]. These devices provide additional damping to the structure, therefore decreasing wind-induced vibrations [12, 13, 14]. While aerodynamic shape modification can generally be employed only for the design of new buildings, modification of the structural system and integration of auxiliary damping devices can be achieved during both the design of new structures and retrofitting of existing buildings. Of interest to this paper is the optimization of the stiffness and passive damping system for wind-induced vibration mitigation.

Some optimization methods for reducing wind-induced vibrations in tall buildings through the modification of the structural system have been proposed. For instance, Chan *et al*. [15] proposed a procedure to find the optimal distribution of the stiffness to achieve serviceability performance. The analysis under wind load was conducted in the frequency domain, and an optimality criteria method was employed to select element stiffness values that satisfied peak acceleration thresholds. Li *et al.* [16] introduced an optimization method for the design of tall rectangular steel buildings. A micro-genetic algorithm was used to select the sizes of the steel structural elements that satisfied lateral drift and acceleration constraints. The authors applied their procedure to a 30-story building exposed to wind load, and showed that their algorithm was able to find an optimal distribution of member sections that guaranteed serviceability performance under wind loads. Other authors studied the integration of supplemental energy dissipation devices in tall buildings for wind-induced vibration mitigation. For instance, [17] proposed an optimal design procedure for active tuned-mass dampers installed in wind-excited tall buildings. The number and the location of the active tuned-mass dampers were optimized to restrict the flexural and torsional accelerations experienced by the building to predefined performance levels. Micheli *et al.* [18] applied a performance-based design (PBD) approach to the design of passive viscous and friction dampers under stochastic wind loads. In their study, damping devices were designed to limit acceleration within the serviceability thresholds. A life-cycle analysis (LCCA) was embedded in the PBD to quantify the economic benefits provided by the integration of passive dampers in a high-rise structure and the LCCA was used as a decision parameter to compare different damping strategies. Later, Micheli *et al.* [51, 52] extended the procedure to tall buildings equipped with high performance control system, including active, semi-active, and hybrid motion control devices. However, few studies can be found in the literature that optimize simultaneously both the structural system and damping device configurations to reduce wind-induced vibrations. One of the major challenges in the development of such optimization procedure is the computational cost of extensive numerical simulations required to optimize the large number of design variables involved in the problem. This aspect is exacerbated when the analysis is conducted in the time domain, given the long excitation time series under consideration in wind analysis.

An alternative approach that has gained popularity in the last few decades is the use of surrogate models, or metamodels, as a solution for computationally expensive simulation problems [19, 20,

21, 22, 23]. A surrogate model is a mathematical representation of the numerical model under consideration, obtained by reconstructing the underlying input-output relationship from a limited set of data. Metamodels have been applied to a variety of engineering fields, including aerospace engineering [24], structural dynamics [25], and uncertainty quantification of stochastic systems [26]. In civil engineering applications, Sudret and May [27] were among the first to propose a polynomial chaos expansion approach to build fragility curves of structures subjected to seismic hazards. Gidaris *et al.* [28] applied a Kriging surrogate model to seismic risk assessment of a 4-story building. In their work, fragility functions parameters were estimated using the Kriging model and considering uncertainties in structural parameters and ground motion characteristics. Gidaris *et al.* [29] tailored an optimization framework based on the Kriging surrogate to the design of a floor isolation system for buildings subjected to seismic loads. Micheli *et al.* [30] evaluated the use of a radial basis function (RBF) metamodel for the risk-assessment of a 39-story building equipped with damping devices. Results demonstrated the promise of the RBF surrogate at estimating the risk of the facility. Micheli *et al.* [31] investigated the use of Kriging surrogate and adaptive wavelet network (AWN) metamodels for the uncertainty quantification of a semi-active control system. The authors concluded that the AWN provided a fast and reliable estimation of the average system response, while the Kriging could be used for a robust design of the control system, later developed in Micheli *et al.* [53]. In all of the surveyed applications, the use of surrogate models as a replacement of the original numerical simulation model yielded a significant reduction in the computational demand for the performed tasks.

In this paper, a novel metamodel-based procedure to optimize the structural system and damping device configurations in tall buildings subjected to wind loads is introduced. In the proposed procedure, Kriging surrogate models are employed to estimate the building response under a large number of structural system and damping device configuration scenarios, reducing the computational demand of the optimization process. The proposed procedure is aimed at designing supplemental damping devices and structural system modifications to provide a balanced and economic solution to reduce the dynamic effects of the wind excitation. The motion design objective of the optimization process is serviceability, and performance is quantified through LCC, which allows to account for costs associated with the structural system modifications and passive damping device integration, along with the savings generated by vibration mitigation projected through the lifespan of the structure. To find the optimal configuration, the building is simulated under a large number of scenarios, and each scenario under a different combination of structural system properties (e.g., floor stiffness) and damping device characteristics (e.g., damper capacity). To avoid computationally demanding simulations, the original computational model is replaced by a set of Kriging surrogate models, each emulating the response of a single floor of the structure. The surrogate models are constructed using a data-driven approach based on a simulated input-output dataset. The response of the building floors, derived with the Kriging metamodels, is then related to the LCC through fragility curves and cost analysis. Note that the building is assumed to have been designed to satisfy wind load design requirements following current code-specified standards (i.e., ASCE 7-16), guaranteeing capacity requirements.

The reminder of the paper is organized as follows. Section 2 gives a brief background on life-cycle cost analysis and introduces the proposed LCC optimization procedure that uses Kriging surrogate models as its computational engine. Section 3 describes case study building, wind load, and cost analysis models. Section 4 presents the Kriging surrogate modeling approach employed in this study. Section 5 discusses the results. Finally, section 6 concludes the paper.

2. Life-Cycle Cost Optimization Methodology

This section introduces the proposed methodology for optimizing structural system and damping device characteristics of tall buildings subjected to wind loads based on the LCC of the structure. A brief description of the LCC analysis is first provided. Then, the proposed surrogate models-based optimization procedure is presented and the metamodeling process adopted in this paper is explained.

2.1 Life-Cycle Cost Analysis Description

The life-cycle cost of a structure equipped with motion control devices can be formulated as [32, 50]:

$$LCC = C_I + C_M + C_F + C_R \tag{1}$$

where C_I is the initial construction cost of the building, C_M is the maintenance cost of structure and damping devices, C_F is the annual failure cost (or the cost of exceeding the set performance objectives), and C_R is the cost of the retrofitting for vibration mitigation, expressed as:

$$C_R = C_{SM} + C_{DV} \tag{2}$$

where C_{SM} is the cost related to structural modifications and C_{DV} is the cost associated with the motion control devices. The cost of failure C_F estimates the economic losses caused by the building not meeting its target performance objectives and can be expressed as:

$$C_F = \sum_{i=1}^{n_t} C_{\text{fail}}(1+r)^{-i\Delta s} \tag{3}$$

where n_t is the lifetime of the structure (in years), r is the interest rate, Δs is the time interval, and C_{fail} is defined as (adapted from [32]):

$$C_{\text{fail}} = \sum_{k=1}^{n_h} P_{h,k}\left[\sum_{j=1}^{n_f}\left(\sum_{l=1}^{n_e}\sum_{m=1}^{n_{DS}} P_{DS,m,l,j} C_{DS,m}\right)\right] \tag{4}$$

where $P_{h,k}$ is the annual probability of occurrence of the k-th wind hazard event, n_h is the total number of hazard events considered in the cost analysis, n_f is the number of floors of the building, n_e is the number of elements (per floor) that can be damaged if the target performance objective is not met, n_{DS} is the number of damage states defined per each element, $P_{DS,m,l,k}$ is the probability of

the m-th damage state to occur in the l-th element of the j-th floor conditional to the k-th wind hazard event occurrence, and $C_{DS,m}$ is the repair costs associated with the m-th damage state. P_h can be estimated from a site-specific wind hazard curve, which expresses the annual probability of occurrence of a wind hazard event characterized by a certain intensity measure (IM) as a function of the building geographic location. P_{DS} represents the probability that a certain structural or nonstructural element will undergo one or more damage states conditional to a certain engineering demand parameter (EDP) value and can be evaluated by combining the structural response of the building expressed in terms of peak floor acceleration (a_{peak}) and maximum story drift ratio (SDR) with fragility curves available in the literature [32]. The procedure for estimating C_{fail} is schematically reported in Fig. 1.

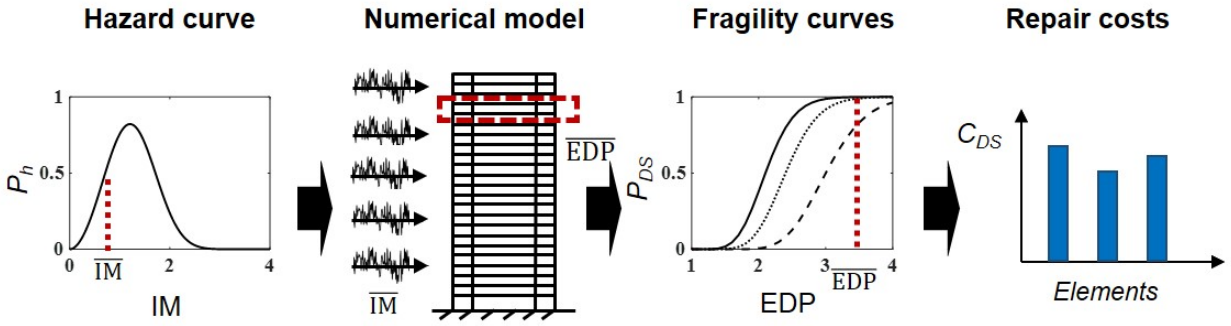

Fig. 1 Schematic representation of the cost of failure estimation process: EDPs (i.e., peak floor acceleration and maximum story-drift ratio) are computed with a numerical model of the building subjected to a wind load characterized by a certain IM; after, the EDPs are combined with fragility curves to assess the damage level of building elements and corresponding economic losses (repair and replacement costs).

2.2 Life-Cycle Cost Optimization Using Surrogate Models

The proposed surrogate models-based procedure is aimed at optimizing the structural system and damping device characteristics with the final goal of minimizing the LCC of the structure. Structural system modifications are modeled as a variation in the stiffness of the building floors. Damping device configurations are modeled using variables representing the total damping force capacity of devices and the number of dampers per floor. The optimization problem can be expressed as:

$$\begin{aligned} &\min_{K_j, F_{\max,j}, n_{D,j}} \quad C_M + C_F + C_R \\ &\text{subj.} K_j \geq K_{j,\text{INI}} \\ &j = 1, \dots, n_f \end{aligned} \tag{5}$$

where the variables to optimize are K_j, the stiffness of the j-th floor, $F_{\max,j}$, the damping capacity of the device at the j-th floor, $n_{D,j}$, the number of damping devices installed at the j-th floor; n_f is the total number of building floors; and $K_{j,\text{INI}}$ is the initial value of the j-th floor stiffness obtained by the preliminary design of the building assuming that the structure was designed to satisfy code-

specified capacity requirements. In Eq. (5), it is assumed that C_I is a constant construction cost associated with the preliminary design of the building, and is thus excluded by the optimization process. The values of K_j, $F_{\max,j}$, and $n_{D,j}$ that minimize the LCC are obtained by simulating the building under a large number of scenarios using a set of Kriging surrogate models, where each scenario is characterized by a different combination of structural system properties (floor stiffness K_j), damping device characteristics (damper capacity $F_{\max,j}$, number of damping devices $n_{D,j}$), and wind load intensities (wind speed acting on the j-th floor V_j). While V_j is not an optimization variable, different values of the wind speed need to be considered in the LCC computation to account for the variability of the wind load intensity during the lifetime of the structure. The proposed procedure is schematically reported in Algorithm 1 and Fig. 2 for a generic n_f-story structure. The first step of Algorithm 1 consists of identifying the possible structural system modifications and damping device locations (i.e., floors) starting from the preliminary design of the building. After, multiple Kriging surrogate models are formulated to emulate the structural response of each floor of the structure based on n observation data (Step 3 of Algorithm 1). The input vector, **x,** of the metamodels is related to the structural system and damping device characteristics (K_j, $F_{\max,j}$, and $n_{D,j}$) as well as to the wind speed (V_j), while the output, **y** ,is associated with the EDPs. Further details on this step are given below. Exploiting the prediction capability of the surrogate models, the EDPs and the LCC are computed for a large number n_V of different K_j, $F_{\max,j}$, $n_{D,j}$, and V_j scenarios (Step 4), and the optimal stiffness-damping configuration is taken as the scenario that minimizes the LCC (Step 5).

Algorithm 1: Proposed LCC optimization procedure with Kriging surrogate models

1:	Identify input variables range of variability based on preliminary design
2:	Create n observation data {**x**, **y**}
3:	for j = 1: n_f
	Train the j-th Kriging metamodel with the j-th floor training observations
	Test the j-th Kriging metamodel accuracy with the j-th floor testing observations
	if the accuracy threshold of the j-th Kriging metamodel is reached
	stop the training
	Else
	increase n
	End
4:	Generate n_v different combinations of **x**
5:	for i =1:n_v
	Predict **y** values with the n_f Kriging metamodels
	Estimate C_{fail}, C_R, and LCC
	end
6:	Find the min of LCC

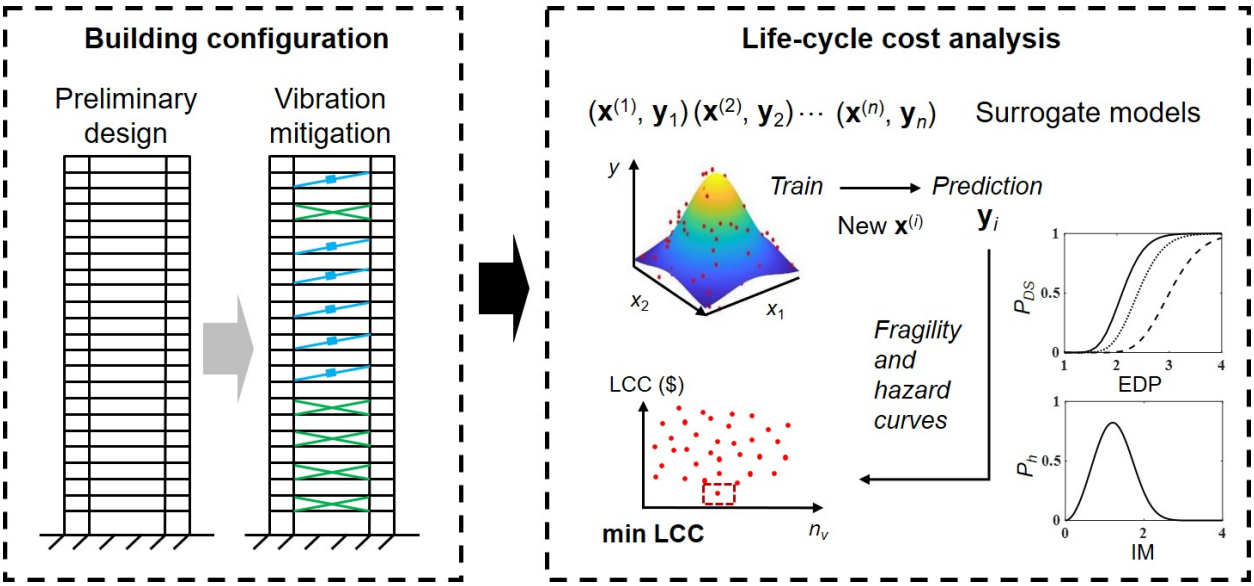

Fig. 2 Representation of the proposed surrogate models-based LCC optimization procedure.

In Step 3 of Algorithm 1, multiple surrogate models are employed as replacement of the original numerical simulation model to reduce the computational demand of the optimization process [49]. A Kriging surrogate model is defined for each floor of the structure. Each surrogate model includes the floor wind speed, structural characteristics, and damping device properties as inputs, and the corresponding EDPs as output. For example, for the generic floor j, the input of the j-th surrogate model is defined as $\mathbf{x} = \{K_j, F_{\max,j}, n_{D,j}, V_j\}^{\mathrm{T}}$. The output of the surrogate is taken as the EDPs of the j-th floor, namely $\mathbf{y} = \{a_{\mathrm{peak},j}, \mathrm{SDR}_j\}$, to be used for the fragility analysis and cost estimation described in Sec. 2.1. The n observations required to train and test the surrogate models are created by numerically simulating the entire building under n different $\mathbf{K}_{SM}$, $\mathbf{F}_{\max}$, $\mathbf{n}_D$, and $\mathbf{V}$ scenarios, where $\mathbf{K}_{SM} = \{K_1, \ldots, K_{nf}\}$, $\mathbf{F}_{\max} = \{F_{\max,1}, \ldots, F_{\max,nf}\}$, and $\mathbf{n}_D = \{n_{D,1}, \ldots, n_{D,nf}\}$ are vectors containing the variables to optimize and $\mathbf{V} = \{V_1, \ldots, V_{nf}\}$ is a vector containing different values of wind speed. Then, the single floor information (i.e., K_j, $F_{\max,j}$, $n_{D,j}$, V_j, $a_{\mathrm{peak},j}$, and SDR_j) are retrieved from each simulation and used as observations. In the testing process, an accuracy threshold is set (e.g., root mean square error < 10%), and the number of training observations n is increased until such threshold is reached. Note that the surrogate model maps the single floor wind speed, stiffness, and damping configuration characteristics to the corresponding structural response. Therefore, for a generic n_f-floor structure, n_f metamodels are formulated. Although a different metamodel is constructed for each floor of the structure, the dependence between consecutive floor observations is embedded in the data since training/testing observations have been generated with a numerical simulation model of the whole building that accounts for the intrinsic dependence between consecutive floors.

Once the n_f metamodels are trained and their accuracy is considered acceptable, the prediction capability of the surrogates is employed to generate the structural response of the building floors for a large number of new scenarios, n_V, characterized by a variety of different values of K_j, $F_{\max,j}$,

$n_{D,j}$, and V_j (Steps 4 to 5 of Algorithm 1). The predicted EDPs are utilized to estimate P_{DS} in Eq. (4) in combination with fragility curves taken from existing databases. C_{fail} is computed with Eq. (4), given a site-specific hazard curve and the economic losses associated with excessive EDPs values, C_{DS}. In the next step, C_{fail} is projected to the lifetime of the structure with Eq. (3). The cost C_R depends on stiffness, damping capacity, and number of damping devices per building floor, and it is calculated for each $\mathbf{K}_{SM}$, $\mathbf{F}_{\max}$, and $\mathbf{n}_D$ combination. Finally, an LCC value for each of the n_v-scenario is computed with Eq. (1), and the optimal solution is taken as the $\mathbf{K}_{SM}$, $\mathbf{F}_{\max}$, and $\mathbf{n}_D$ combination that minimizes the LCC, as schematically represented in Fig. 2. Note that more constraints can be potentially added to the optimization problem described by Eq. (5) to consider more complex structural systems and to account for constructability aspects.

The Kriging mathematical algorithm used to learn the unknown relationship between input **x** and output **y** in Step 3 of Algorithm 1 is described in Sec. 4.

3. Application to the Case Study Building

This section introduces the case study building, wind load simulation method, and cost models used in this study.

3.1 Simulated Building Model

The case study building is an existing 39-story office tower, located in Boston. The structure is a steel moment-frame system, with an octagonal plan and a total height of 163 m. The inter-story height is set equal to 7.4 m at the ground and roof levels, and 3.9 m at all the other floors. This office tower was selected as a case study because previous research showed that the building was sensitive to wind excitations, experiencing large acceleration levels under frequent wind loads [33]. The building was consequently equipped, during the structural design process, with a set of passive viscous dampers for wind-induced vibration reduction [34]. This structure constitutes of an opportunity to apply the surrogate models-based procedure and compare the preliminary design with the damping/stiffness configuration identified by the proposed LCC optimization method.

The structure is simulated in its weak direction as a spring-dash lumped mass system with the state-space formulation. The equation of motion for the 39-story building can be expressed as [35]:

$$\mathbf{M}\ddot{\mathbf{x}} + \mathbf{C}\dot{\mathbf{x}} + \mathbf{K}\mathbf{x} = \mathbf{E}_w\mathbf{W} - \mathbf{E}_f\mathbf{F} \tag{6}$$

where $\mathbf{x} \in \mathbb{R}^{39\times1}$, $\dot{\mathbf{x}} \in \mathbb{R}^{39\times1}$, $\ddot{\mathbf{x}} \in \mathbb{R}^{39\times1}$ are displacement, velocity, and acceleration vectors, respectively, $\mathbf{W} \in \mathbb{R}^{39\times1}$ is the wind load vector, $\mathbf{F} \in \mathbb{R}^{15\times1}$ is the damping force vector (15 damper sets are installed along the weak direction of the building), $\mathbf{E}_w \in \mathbb{R}^{39\times39}$ is the load location matrix, $\mathbf{E}_f \in \mathbb{R}^{39\times15}$ is the damping force location matrix, $\mathbf{M} \in \mathbb{R}^{39\times39}$, $\mathbf{C} \in \mathbb{R}^{39\times39}$, and $\mathbf{K} \in \mathbb{R}^{39\times39}$ are mass, damping, and stiffness matrices, respectively. The state space model is expressed as:

$$\dot{\mathbf{X}} = \mathbf{A}\mathbf{X} + \mathbf{B}_w\mathbf{W} - \mathbf{B}_f\mathbf{F} \tag{7}$$

where $\mathbf{X} = [\mathbf{x}\ \dot{\mathbf{x}}]^T$ is the 78 × 1 state vector, $\mathbf{A}$, $\mathbf{B}_w$ and $\mathbf{B}_f$ are constant matrices given by:

$$\mathbf{A} = \begin{bmatrix} \mathbf{0} & \mathbf{I} \\ -\mathbf{M^{-1}K} & -\mathbf{M^{-1}C} \end{bmatrix}_{78 \times 78} \tag{8}$$

$$\mathbf{B}_w = \begin{bmatrix} \mathbf{0} \\ \mathbf{M^{-1}E}_w \end{bmatrix}_{78 \times 39} \tag{9}$$

$$\mathbf{B}_f = \begin{bmatrix} \mathbf{0} \\ \mathbf{M^{-1}E}_f \end{bmatrix}_{78 \times 15} \tag{10}$$

Eq. (7) is solved using the discrete form of the Duhamel integral [35]:

$$\mathbf{X}(t + \Delta_t) = \mathbf{X}(t) + \mathbf{A}^{-1}[\exp(\mathbf{A}\Delta_t) - \mathbf{I}]\left[\mathbf{B}_w\mathbf{W}(t) - \mathbf{B}_f\mathbf{F}(t)\right] \tag{11}$$

where Δt is the simulation time interval (taken as 0.01 s) and $\mathbf{I} \in \mathbb{R}^{39\times39}$ is the identity matrix. The inter-story drift is expressed as $\delta_1 = x_1$ at the first floor and $\delta_j = x_j - x_{j-1}$ at the other floors. Table 1 reports the dynamic properties of the building used for **M**, **C**, and **K** [36]. Fig. 3 (a) illustrates a schematic representation of the building equipped with viscous dampers under wind load, which is taken as a preliminary configuration for the application of the proposed optimization procedure.

The damping system of the building is shown in Fig. 3 (a) and consists of 15 sets of two damping devices installed at every other floor, starting from the 5th floor up to the 33th floor, following the location of the existing passive viscous dampers system in the case study building. Each set of devices is simulated as a single device with double the capacity. The force exerted from a viscous damper is simulated as:

$$F_v = c_v \mathrm{sgn}(\dot{u}) \tag{12}$$

where c_v represents the damping coefficient, and $\dot{u}$ is the relative velocity, and $\mathrm{sgn}(\dot{u})$ is the signum function that denotes the sign of $\dot{u}$. The preliminary damping coefficients are taken as 52,550 kN·s/m for the dampers below the 26th floor, and 35,000 kN·s/m for the devices above the 26th floor, and the corresponding damping capacities $F_{\max}$ as 1,350 kN and 900 kN [12].

3.2 Wind Load Simulation Model

The wind force vector **W** in Eq. (6) contains the along-wind fluctuating forces acting on the building floors in the simulated direction, representing the dynamic wind load. The wind force W_j at the j-th floor is taken as [37]:

$$W_j = \rho c_D A_j \left(V_{m,j} + V_{t,j}\right) \tag{13}$$

where ρ is the air density (ρ=1.25 kg/m^3), c_D is the drag coefficient (c_D = 1.5), A_j is the projected area of the building normal to the wind flow, $V_{m,j}$ is the mean wind speed, and $V_{t,j}$ is the fluctuating

wind velocity generated by the wind turbulence. The mean wind speed at the j-th floor can be expressed through a logarithmic law [37]:

$$V_{m,j} = V_{m,10} \frac{\ln(z/z_0)}{\ln(10/z_0)} \tag{14}$$

where z is the reference height above the ground, $V_{m,10}$ is the mean wind speed at z = 10 m, and z_0 is the terrain roughness (z_0 = 0.03 m). The fluctuating wind speed $V_{t,j}$ is simulated using the spectral approach proposed by [38] and it is outlined in [31]. As an example, Fig. 3 (b) plots typical wind force time histories acting on the last floor of the structure for two different values of $V_{m,10}$. The mean wind speed at a reference height of z = 10 m, $V_{m,10}$, is taken as *IM*, since it is the reference velocity for the wind load time series generation in Eq. (13) and Eq. (14) for extension.

Table 1 Dynamic parameters of the simulated building

floor	mass (t)	stiffness (kN/m)	damping (kN·s/m)	floor	mass (t)	stiffness (kN/m)	damping (kN·s/m)
39	125	13206	194	19	948	1414101	20481
38	903	61570	915	18	948	1542103	22332
37	948	144156	2112	17	948	1671516	24204
36	948	200943	2928	16	948	1704402	24680
35	948	429995	6246	15	948	1736539	25145
34	948	668236	9692	14	948	1848105	26758
33	948	688855	9990	13	948	1954807	28302
32	948	707994	102667	12	948	1987942	28781
31	948	721919	10468	11	948	2024855	29315
30	948	788614	11433	10	948	2283559	33057
29	948	866126	12554	9	948	2536604	36717
28	948	880965	12769	8	948	2579392	37336
27	948	889946	12899	7	948	2615282	37855
26	948	959764	13909	6	1482	2662444	38552
25	948	1030839	14937	5	1394	3226434	46708
24	948	1049684	15209	4	1394	3919347	56731
23	948	1064386	15422	3	2295	3929345	56900
22	948	1216929	17620	2	3150	2751949	39892
21	948	1370469	19849	1	1671	2193660	31776
20	948	1385321	200647				

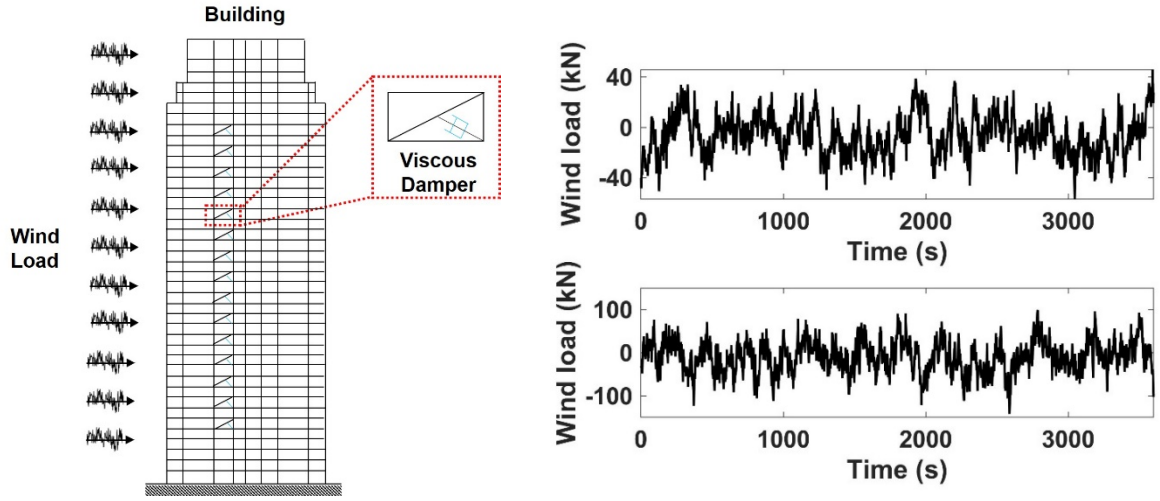

(a) (b)

Fig. 3 (a) Case study building with viscous dampers; (b) wind load time histories at the last floor of the structure for $V_{m,10}$= 18 m/s and $V_{m,10}$= 28 m/s (time interval 0.01 s, duration 3600 s).

3.3 Life Cycle Cost Model

The costs associated with damage states, $C_{DS,}$ in Eq. (4) are associated with the economic losses caused by building occupants' discomfort and damage to nonstructural elements caused by wind-induced vibrations. In what follows, the costs C_{DS} are expressed in USD per wind event. The probability of experiencing a certain damage state, P_{DS}, is estimated using two sets of fragility curves. The first group is composed of peak acceleration-related fragility curves, associated with the probability of experiencing wind-induced discomfort under a certain peak acceleration a_{peak}. In tall buildings, wind-induced accelerations are responsible for motion sickness, sopite syndrome, nausea, sleepiness, and loss in concentration, which can cause indirect economic losses associated with loss in working productivity of the building occupants [39, 40]. Three fragility curves are defined, and associated with three damage states (n_{DS} = 3), representing the increase of severity of discomfort and motion sickness with increasing a_{peak}. These curves are reported in Fig. 4 (a), along with the associated C_{DS}. The values of C_{DS} are estimated based on the assumption that the mean loss in productivity is caused by wind adverse effects (e.g., motion sickness, nausea, fear, sleepiness) is equal to 30% per person [40] and that higher levels of acceleration correspond to higher percentages of building's occupants affected. In Fig. 4 (a), three different percentage of floor occupants perceiving the motion, P_E, are associated with the three fragility curves: P_E = 25% (a quarter of the floor occupants feel the motion) for DS_1, P_E = 50% (half of the floor occupants feel the motion) for DS_2, and P_E = 75% (three quarter of the floor occupants feel the motion) for DS_3. More details on the cost model can be found in Micheli *et al.* [18].

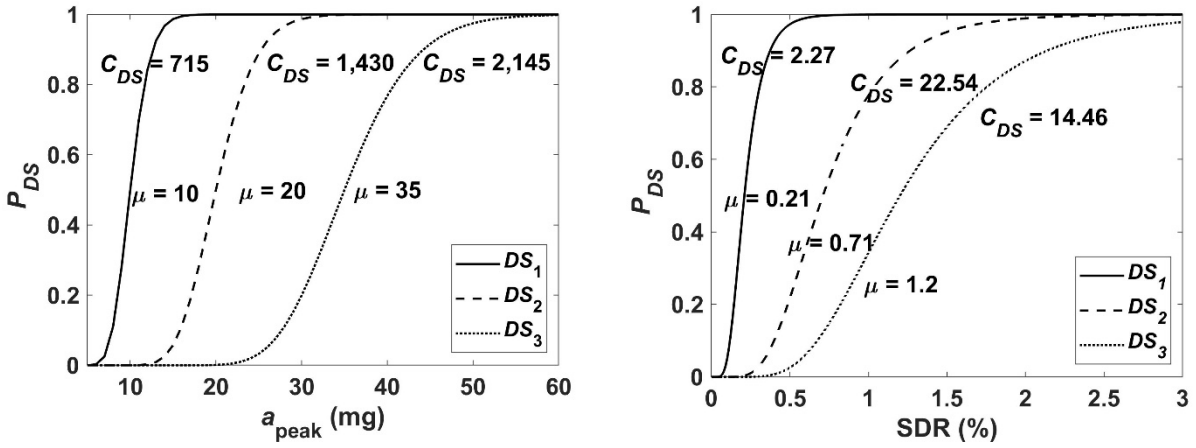

(a) (b)

Fig. 4 Fragility curves: (a) peak acceleration-related fragility curves representing the effects of motion sickness on the building occupants. Lognormal curves with identical standard deviation of 0.12 and individual means μ. The costs are expressed in USD; (b) maximum story-drift ratio related fragility curves associated with the damage to a gypsum partition wall. Lognormal curves with identical standard deviation of 0.45 and individual means μ. The costs are expressed in USD per sf.

The second set of fragility curves are associated with the maximum story drift ratio (SDR). These fragility curves represent the damage experienced by nonstructural components, including glass panels composing the building envelope and internal partitions, during a wind event [41, 42, 43]. In absence of experimental data for wind-induced damage, the fragility curves reported in FEMA-P-58 for earthquake excitation are employed, along with the costs required to repair or replace the damaged components [32]. As an example, Fig. 4 (b) reports SDR-related fragility curves for gypsum partitions, characterized by three damage states ($n_{DS} = 3$) related to the SDR: DS_1, minor cracking of wall board, DS_2, moderate cracking of wall, and DS_3, significant cracking of wall.

Variable P_h in Eq. (4) is taken as the annual probability of occurrence of a wind hazard event characterized by a mean wind speed at z = 10 m above the ground wind speed $V_{m,10}$. Such probability is estimated based on the wind hazard curve reported in Fig. 5. This hazard curve was obtained by fitting a Weibull distribution to meteorological data collected for the area of Boston (MA) [18]. The hazard curve was discretized in n_h = 28 intervals to consider the wide range of wind speed values that the structure can experience during its lifespan.

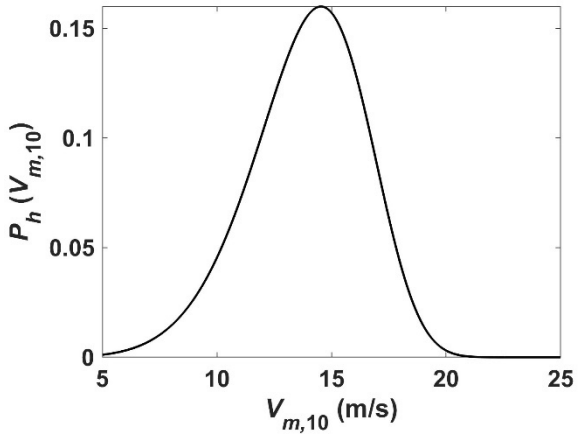

Fig. 5 Wind speed hazard curve for the 39-story building located in Boston Represented by Weibull distribution with scale parameter 14.9 and shape parameter 6.4.

The cost (in USD) of the dampers C_{DV} in Eq. (2) depends on capacity and number of damping devices per floor, and it is taken as [44]:

$$C_{DV} = [0.77(F_{\max})^{1.207} + 2806]n_D \tag{15}$$

The structural system modification cost, $C_{SM,}$ depends on the solution adopted to increase the stiffness of the system. In absence of cost data related to the increase of stiffness in a structural system, a parametric study is conducted by assuming three different values of C_{SM}, representative of different levels of structural modification. In case 1, C_{SM} is assumed as 10,000 USD, in case 2, C_{SM} = 25,000 USD, and in case 3, C_{SM} = 50,000 USD per building floor. The cost analysis is repeated for these three cases.

In Eq. (1), the initial construction cost of the building is taken as C_I = 177.84 USDM, considering an average price of 2,100 USD per square meter and a total building area of 82,612 m^2 (Micheli *et al.* 2019 a). No maintenance costs are considered for the dampers and for the structural system, so C_M = 0 (retrieved from [45]). Finally, in Eq. (3), the lifetime of the structure is taken as 50 years, r is assumed as 3%, and Δs as 1 year. Note that the interest rate depends on the building location and could be set to a different value.

4. Surrogate Model

In this section the Kriging metamodel algorithm is described, along with the optimization variables employed as inputs for the surrogate.

4.1 Kriging Algorithm

The metamodeling process, described in Sec. 2, consists of creating multiple Kriging surrogate models to emulate the structural response of each floor of the structure based on a set of input/output observations. Here, it assumed that the structural response (EDPs) of each floor of the building derives from an independent stochastic process, $Y(\mathbf{x})$. Following the Kriging formulation

[46] for a generic system with input **x** and scalar output y, a stochastic process can be described as:

$$Y(\mathbf{x}) = \mu(\mathbf{x}) + Z(\mathbf{x}) \tag{16}$$

where $\mu(\mathbf{x})$ is the mean of the process and $Z(\mathbf{x})$ is the deviation from the mean, assumed to follow a Gaussian distribution with zero mean and covariance matrix, **V**:

$$\mathbf{V} = \sigma^2 \mathbf{\Psi} \tag{17}$$

where σ^2 is the variance of the process, and $\mathbf{\Psi} \in \mathbb{S}_{++}^{n \times n}$ is the correlation matrix for n realizations:

$$\mathbf{\Psi} = \begin{bmatrix} \psi\left[Y\left(\mathbf{x}^{(1)}\right), Y\left(\mathbf{x}^{(1)}\right)\right] & \cdots & \psi\left[Y\left(\mathbf{x}^{(1)}\right), Y\left(\mathbf{x}^{(n)}\right)\right] \\ \vdots & \ddots & \vdots \\ \psi\left[Y\left(\mathbf{x}^{(n)}\right), Y\left(\mathbf{x}^{(1)}\right)\right] & \cdots & \psi\left[Y\left(\mathbf{x}^{(n)}\right), Y\left(\mathbf{x}^{(n)}\right)\right] \end{bmatrix} \tag{18}$$

with the Gaussian correlation function ψ expressed as:

$$\psi\left[Y\left(\mathbf{x}^{(p)}\right), Y(\mathbf{x}^{q})\right] = \exp\left(-\sum_{s=1}^{k} \theta_s \left| x_s^{(p)} - x_s^{(q)} \right|^2 \right) \tag{19}$$

where $Y(\mathbf{x}^{(p)})$, $Y(\mathbf{x}^{(q)})$, $p, q = 1, \ldots, n$ are realizations of the stochastic process, k is the number of input variables, and θ_s, $s = 1, \ldots, k$ are the hyper-parameters of the correlation function. The hyper-parameters of the Kriging function can be identified using the maximum likelihood method [46]. The Gaussian likelihood function, L, can be written as a function of the sample data **y**:

$$L = \frac{1}{(2\pi\sigma^2)^{n/2} |\mathbf{\Psi}|^{1/2}} \exp\left[-\frac{(\mathbf{y} - \mathbf{1}\mu)^{\mathrm{T}} \mathbf{\Psi}^{-1} (\mathbf{y} - \mathbf{1}\mu)}{2\sigma^2} \right] \tag{20}$$

The hyperparameters that maximize the likelihood, L, are [46]:

$$\hat{\sigma}^2 = \frac{1}{n} (\mathbf{y} - \mathbf{1}\mu)^{\mathrm{T}} \tilde{\mathbf{\Psi}}^{-1} (\mathbf{y} - \mathbf{1}\mu) \tag{21}$$

$$\hat{\mu} = \frac{\mathbf{1}^{\mathrm{T}} \mathbf{\Psi}^{-1} \mathbf{y}}{\mathbf{1}^{\mathrm{T}} \mathbf{\Psi}^{-1} \mathbf{1}} \tag{22}$$

where the hat denotes an estimate, and $\mathbf{1} \in \mathbb{R}^{n \times 1}$ is a column vector of ones. In this study, a genetic algorithm is employed to maximize Eq. (20) and find the unknown hyperparameters. After, the Kriging surrogate can be used to predict the output $\hat{y}$ from a new sample **x**. First, the vector $\tilde{\mathbf{y}} = \{\mathbf{y}^{\mathrm{T}}, \hat{y}\}^{\mathrm{T}}$ is created, then correlation matrix is augmented with the new sample **x** [46]:

$$\tilde{\mathbf{\Psi}} = \begin{bmatrix} \mathbf{\Psi} & \boldsymbol{\psi}_w \\ \boldsymbol{\psi}_w^{\mathrm{T}} & \mathbf{1} \end{bmatrix} \tag{23}$$

where $\boldsymbol{\psi}_w$ is the vector of correlations between the observed data $\mathbf{y}$ and the new prediction $\hat{y}$, computed using Eq. (19). Then, the likelihood function is augmented with the new $\widetilde{\boldsymbol{\Psi}}$ and $\tilde{\mathbf{y}}$, and the maximum likelihood method is applied. It can be shown that the maximum likelihood estimate for $\hat{y}$ is given by:

$$\hat{y}(\mathbf{x}) = \hat{\mu} + \boldsymbol{\psi}_w^{\mathrm{T}} \boldsymbol{\Psi}^{-1} (\mathbf{y} - \mathbf{1}\hat{\mu}) \tag{24}$$

Eq. (24) can be employed to estimate outputs y from new samples $\mathbf{x}$. Note that when two samples are very close to each other, the nearest symmetric positive matrix is used for $\boldsymbol{\Psi}$ [47] to prevent the correlation matrix in Eq. (19) from becoming poorly conditioned.

4.2 Inputs of the Surrogate Models

A total of $n_f = 39$ surrogate models are created to emulate the structural response of the building floors. In order to identify suitable design variables, it is assumed that the structural system configuration described in Sec. 3.1 and schematically represented in Fig. 3(a), including viscous dampers locations, capacities, and stiffness, is the first design iteration (i.e., preliminary design) of the building. The inputs of the surrogate models are taken as wind speed, structural characteristics and damping device characteristics, and the corresponding peak floor acceleration, a_{peak}, and maximum story-drift ratio, SDR, as outputs. Specifically, the first input variable of the j-th metamodel is the mean wind speed at the j-th floor, $V_{m,j}$, calculated with Eq. (14) based on $V_{m,10}$. The second variable of the input vector is the floor stiffness K_j, and it is related to possible structural modifications made to reduce wind-induced vibrations. The third and fourth variables are related to the integration of motion devices, and are given by damping capacity, $F_{\max,j}$, and number of devices, $n_{D,j}$, at the j-th floor. Because in the preliminary design of the building the dampers are installed each other floor, it is necessary to distinguish between controlled (floors with dampers) and uncontrolled floors (floors without dampers). For the generic controlled floor j, the input of the surrogate model can be written as $\mathbf{x} = \{V_{m,j}, K_j, F_{\max,j}, n_{D,j}\}^{\mathrm{T}}$ and $k = 4$. For the generic uncontrolled floor j, the input of the surrogate model is $\mathbf{x} = \{V_{m,j}, K_j\}^{\mathrm{T}}$ and $k = 2$. The outputs of the j-th surrogate are taken $a_{\text{peak},j}$ and SDR_j which represent the peak acceleration and maximum story-drift ratio experienced by the j-th floor of the structure.

The ranges of variability of the input variables of the surrogate models are reported in Table 2. The speed $V_{m,10}$ is varied between 5 and 28 m/s, in order to represent the range of the wind speeds that the structure will likely experience during its lifetime (hazard curve in Fig. 5). Wind load time histories are generated based on the values of $V_{m,10}$. Then, for each time series the mean wind speed $V_{m,j}$ is calculated using Eq. (14). The range of variability of the other input variables is selected based on the nominal values of stiffness and viscous dampers reported in Sec. 3.1. Specifically, the stiffness of the system is increased, while the damping characteristics are decreased to find an optimal balance between structural system modifications and damping devices integration. The stiffness K_j, is increased up to 25 % of its nominal value (Table 1) to represent an increase of stiffness designed to reduce wind-induced motion. Such increase of stiffness can be attained modifying the structural system with the augmentation of bracing systems, retrofitting existing braces, or modifying the structural connections. The damping capacity, $F_{\max,j,}$ is decreased by up

to 50% of its nominal value, while the number of damping devices $n_{D,j}$ is varied between 0 and 2. These range values have been selected to avoid numerical instabilities in the simulation model of the building with dampers.

Table 2: List of input variables and the associated range of variability.

Variable	Symbol	Range of variability
Mean wind speed	$V_{m,10}$	5 – 28 (m/s)
Stiffness	K_j	$K_j \cdot [1.0, 1.25]$
Damping capacity	$F_{\max,j}$	$F_{\max,j} \cdot [0.5, 1.0]$
Number of dampers	$n_{D,j}$	[0, 2]

The observation data set for the metamodeling process is created by randomly sampling the inputs from their range of variability in Table 2 with the space-filling Latin Hypercube Sampling (LHS) method and simulating the system with Eq. (7) to (11). The n observations are divided into two subsets: the training subset, with size n_{tr}, and the testing subset, with size n_{ts} ($n = n_{tr} + n_{ts}$). The testing data set size is taken as $n_{ts} = 0.25\ n$ [46]. The training samples are employed to learn the underlying function $\mathbf{y} = f(\mathbf{x})$ that converts the input vector $\mathbf{x}$ into output $\mathbf{y}$, while the testing data are used to verify the accuracy of the metamodel. In this paper, the training process starts with $n_{tr} = 100$ observations and continues until a pre-selected accuracy threshold is reached.

5. Surrogates-based Optimization Results

This section presents the results of the proposed optimization procedure applied to the case study building. First, the Kriging surrogate model accuracy is assessed using the root mean square error (RMSE) as the performance metric. Second, the LCC results are presented, along with the resulting optimal stiffness, damping coefficients, and number of devices per floor.

5.1 Kriging Surrogate Accuracy

The RMSE is utilized to estimate the prediction accuracy of the surrogate models, defined as:

$$\mathrm{RMSE} = \sqrt{\frac{\sum_{i=1}^{n_t}(y_i - \hat{y}_i)^2}{n_t}} \tag{25}$$

where $\hat{y}_i$ is the maximum acceleration estimated by Kriging surrogate model, and y_i is the true maximum acceleration obtained from numerical simulations. The RMSE is normalized with respect to the difference between maximum and minimum values of the testing data set [46]. The accuracy threshold in Algorithm 1 is taken as RMSE ≤ 10 % and the training data set size, n_{tr}, is increased of 100 samples until the RMSE converges. The RMSE of the Kriging metamodels are shown in Fig. 6, as a function of the building floors and training data set size, n_{tr}.

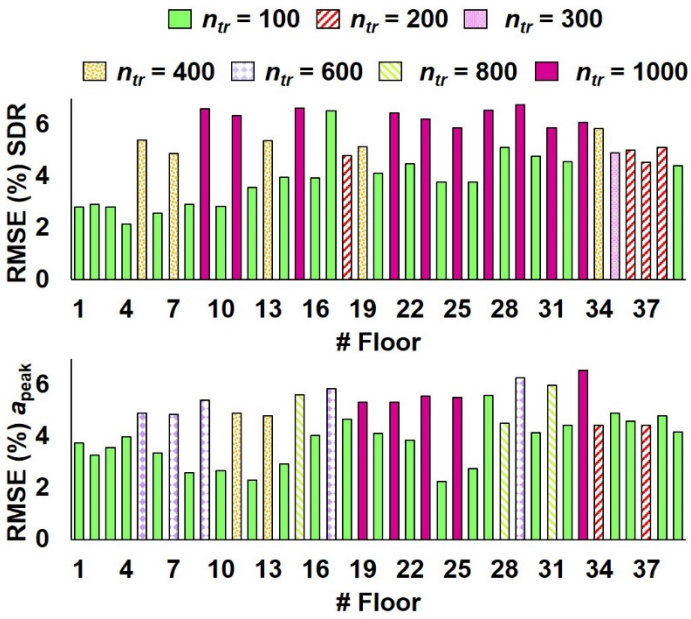

Fig. 6 RMSE as a function of the building floors for SDR and a_{peak}.

Results in Fig. 6 show that the RMSE is higher for the floors equipped with dampers (installed at each other floor starting from the 5th up to the 33rd floor), attributable to the more complex structural behavior. This could be attributed to the larger number of input variables (k = 4) associated with the controlled floors than the uncontrolled ones (k = 2). The size of the training data set varies from 100 to a maximum of 1,000 samples. For the SDR, the majority of the metamodels corresponding to the uncontrolled floors reached an RMSE ≤ 10 % after 100 or 200 samples, while for the controlled floors 1,000 samples were necessary to attain an acceptable accuracy. Similar results can be observed for a_{peak}, where the majority of the metamodels corresponding to the uncontrolled floors reached an acceptable accuracy with 100 samples, while surrogates corresponding to the controlled floors required a larger number of samples. As an example, Fig. 7 reports the trend of the RMSE versus the training data set size for SDR and a_{peak}, and for metamodels corresponding to four different floors of the building. One can notice that the RMSE tends to converge after a certain number of samples. This behavior is observed for both SDR and a_{peak}.

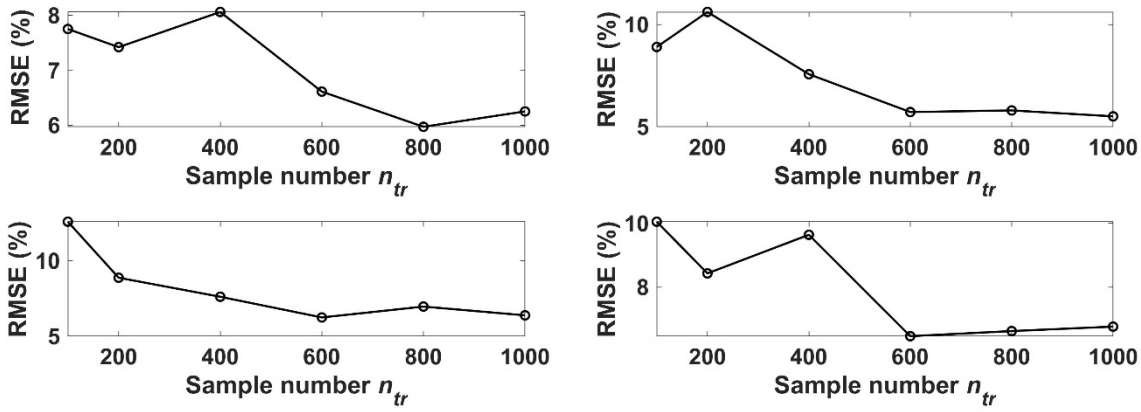

Fig. 7 RMSE convergence plots for: (a) SDR, floors 31 (upper) and 33 (lower); (b) a_{peak}, floors 21 (upper) and 29 (lower).

5.2 Optimization Results

The prediction capability of the surrogate models is employed to predict the output (SDR and a_{peak}) for n_v = 2,000 different combinations of inputs **x**. The range of variability of the input variables is the same as that used for training the surrogate models (Table 2) except for the mean wind speed that was sampled directly from the hazard curve reported in Fig. 5 using the LHS method. The output of the n_v different scenarios were then utilized to estimate the cost of failure C_F and the LCC. Note that a different cost C_R corresponds to each stiffness-damper scenario, given by the different cost of the dampers and stiffness integration. The results of the analysis are illustrated in Fig. 8. The figure reports histograms representing the frequency of the costs C_F, C_R, and their sum over the n_v = 2,000 iterations, for the three C_{SM} cases considered in this study. Comparing the histograms of C_F and C_R in the three cases, one can notice that in case 1, C_R is lower than C_F, in case 2 C_R is similar to C_F, and in case 3 C_R is larger than C_F. This is attributed to the higher value assumed for C_{SM}, which increases from case 1 to case 3. The results indicate that when C_{SM} is large, it might not be economically convenient to increase the stiffness of the system because the cost of structural system modification overcomes the costs of exceeding performance objectives (i.e, failure costs) projected on the lifetime of the structure. Conversely, a fair balance between failure costs and mitigation system cost is reached in case 2, where C_{SM} is 25,000 USD. A comparison between the three cases shows that case 1 leads to the lowest values of the sum C_F and C_R, and therefore to the smallest LCC.

The sum of the costs C_F and C_R, shown in Fig. 8 (c), (f), and (i), are then taken as LCC, since C_M = 0 and C_I is the constant value of the preliminary design building (not part of the optimization process). The stiffness-damper scenarios that lead to the minimum LCC are identified for each case, and the corresponding stiffness-dampers configuration is extracted. The minimum LCC values are equal to 1.30 USMD in case 1, 2.16 USMD in case 2, and 5.38 USMD in case 3. Results in terms of stiffness and damping devices are reported in Fig. 9 and Table 3. Fig. 9 illustrates the optimized stiffness configuration of the building for the three C_{SM} cases, along with the stiffness of the preliminary configuration (values listed in Table 1). One can observe that the stiffness configuration is similar for the three cases, with case 3 slightly lower than the other two cases. It

can also be noticed that the difference between stiffness in the initial and optimized configurations is larger on the lowest floor than on the top floors, and tends to decrease with height. Table 3 reports the damping device characteristics corresponding to the optimal solutions. Comparing the three cases, it can be observed that the number of devices and controlled floors tend to increase from case 1 to 3. This could be attributed to the increasing values of C_{SM} in the three cases. For example, one can note that in case 3 the optimal stiffness profile is lower than in case 1 (Fig. 9), while the number of viscous dampers is larger. A cross-comparison with the initial damping configuration (Sec. 3.1) shows that a lower number of dampers, with lower $F_{\max}$ values, is necessary to minimize the LCC.

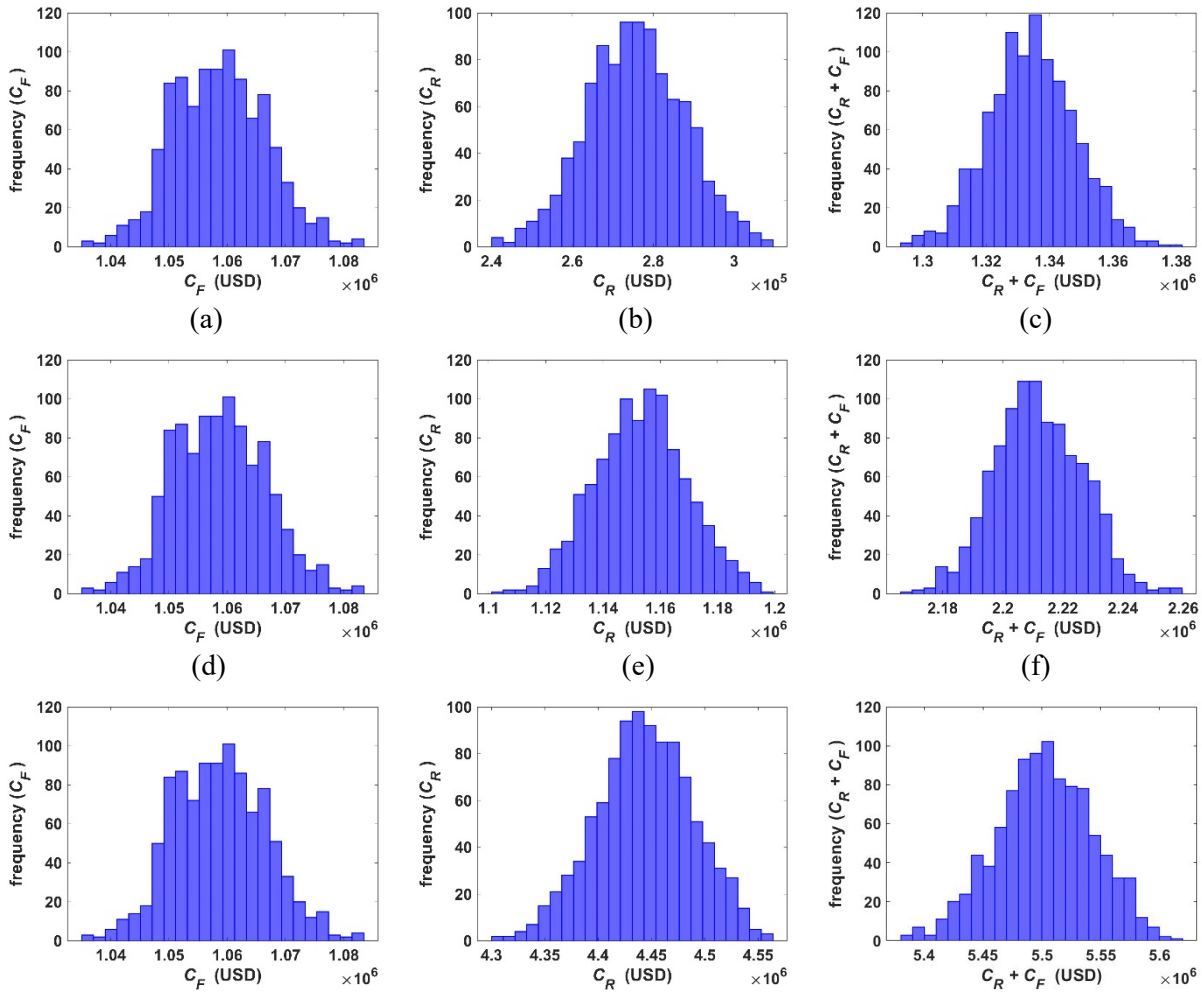

Fig. 8 Histograms summarizing the cost results of n_v = 2,000 scenarios: (a) cost of failure, case 1; (b) cost of the wind-induced vibration mitigation system, case 1; (c) sum of cost of failure and cost of the wind-induced vibration mitigation system, case 1; (d) cost of failure, case 2; (e) cost of the wind-induced vibration mitigation systems, case 2; (f) sum of cost of failure and cost of the wind-induced vibration mitigation systems, case 2; (g) cost of failure, case 3; (h) cost of the wind-induced vibration mitigation system, case 3; (i) sum of cost of failure and cost of the wind-induced vibrations mitigation system, case 3.

Table 3 Optimal damping devices configuration for the three C_{SM} cases

Case	Floor	F_{max} (kN)	n_D
1	11th	1,200	1
	13th	1,200	1
	19th	1,300	1
	27th	800	1
	31st	800	2
2	5th	1,200	1
	9th	1,200	1
	13th	1,200	1
	15th	800	2
	25th	800	1
	27th	800	1
	29th	800	1
	31st	800	1
3	11th	800	2
	13th	800	1
	17th	1,000	2
	19th	1,000	1
	21st	1,000	1
	23rd	1,000	1
	25th	1,000	2
	27th	800	1
	31st	800	1
	33rd	800	1

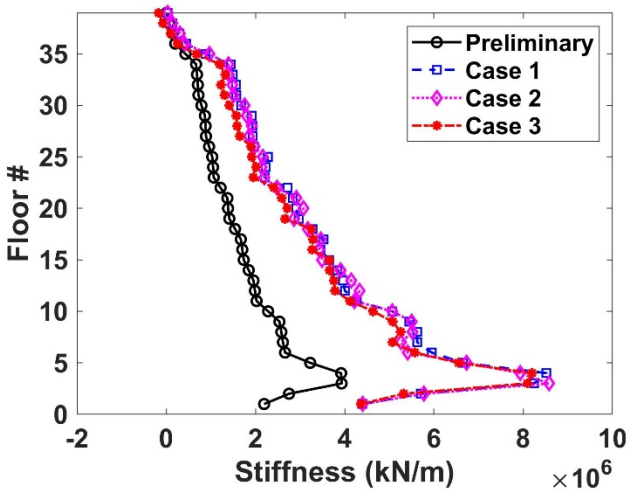

Fig. 9 Optimal stiffness configuration for the three C_{SM} cases.

A comparison between the peak accelerations predicted by the Kriging metamodels and by the simulation model as a function of optimal stiffness and damping device configurations was carried out for further validation. Fig. 10 plots the results for the three cases over a wind speed of 23 m/s, showing that the Kriging metamodels yielded similar peak acceleration values than the simulation model for the majority of the floors for all cases. One can also notice that the simulation model led to a smoother acceleration profile than the Kriging surrogate models. This difference can be attributed to the RMSE values associated with the metamodels over some of the floors as described in Sec. 5.1.

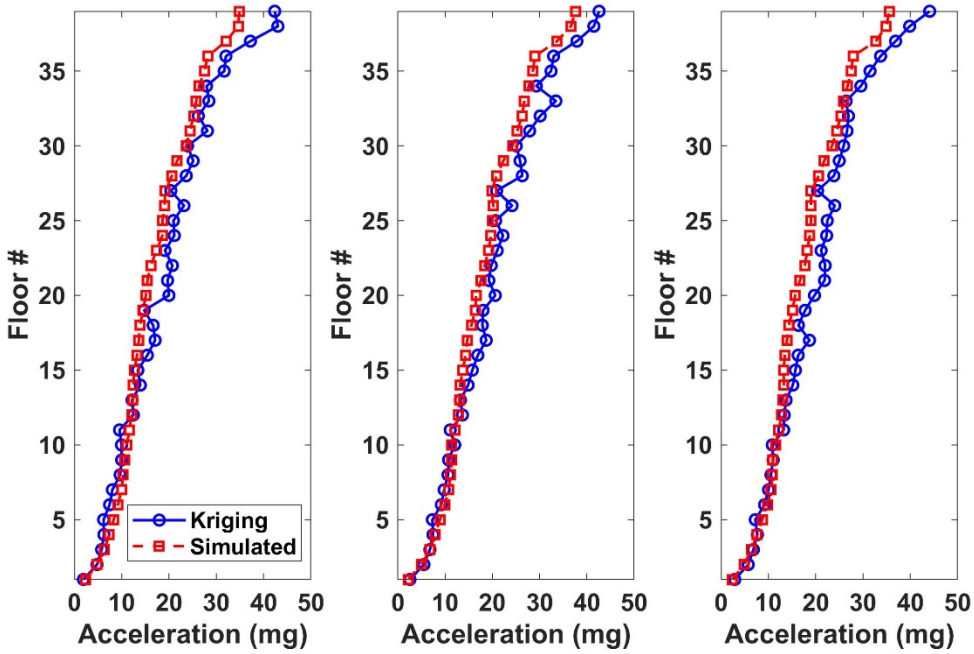

(a) (b) (c)

Fig. 10 Comparison between peak accelerations predicted with the Kriging metamodels and the simulation model for a wind speed $V_{m,10}$ equals to 23 m/s in (a) case 1; (b); case 2; (c) case 3.

6. Conclusions

In this paper, a surrogate models-based optimization procedure to optimize structural system and damping devices characteristics of wind-excited tall buildings was introduced. The objective of the proposed procedure was to find an optimal combination of structural system modifications and damping devices integration to minimize the life-cycle cost (LCC) of the structure, ensuring an acceptable performance of the building in terms of building occupants' comfort and non-structural damage prevention. A set of Kriging surrogate models was employed as a replacement of the original numerical simulation model to reduce the computational effort of the analysis carried out in the time domain. The metamodels were built to emulate the structural response of the building floors using a data-driven approach based on simulated input-output observations. The

performance of the building was then expressed in terms of LCC to consider the initial economic investments in structural system modifications and damping devices integration, along with the lifetime savings in vibration mitigation given by their addition in the structural system. A large number of different scenarios, representing different combinations of structural system and damping device characteristics were considered. The LCC was estimated for each scenario with the Kriging metamodels, and the combination of structural system and damping devices characteristics that minimized the LCC was taken as optimal solution.

A wind-sensitive 39-story building equipped with a set of 15 damping devices and exposed to wind load time histories was taken as case of study. A metamodel for each building floor was constructed to emulate peak floor acceleration (a_{peak}) and maximum story-drift ratio (SDR), for a total of 39 surrogate models. The inputs of the metamodels were wind speed, floor-stiffness, maximum damping capacity, and number of dampers. Results in terms of metamodels accuracy demonstrated that the root mean squared error was higher for the floors equipped with dampers than for the floors without damping devices. This was attributed to the larger number of input variables of the surrogates associated with the floors equipped with dampers than the floors with no dampers. In terms of LCC, results demonstrated that in order to minimize the LCC of the structure, it was necessary to increase the stiffness of the building and decrease the number of dampers in some controlled floors in comparison with the preliminary design of the building. Furthermore, the results of a parametric study on the costs of the structural system modification demonstrated that the optimal stiffness-damping device configuration was dependent on the cost assumed for the stiffness variation.

Overall, this paper showed that using surrogate models is a viable solution for finding a balance between structural system modifications and damping devices integration to reduce wind induced vibrations in wind-excited tall buildings. While the feasibility of the proposed method was demonstrated, the applicability of the results is limited to the space domain considered, like any other metamodeling approach, here relating to the building's preliminary design and location. Future work will study the application of the proposed method to different damping devices and structures that exhibit nonlinear behavior and to more complex structural systems.

Acknowledgements

This paper is based upon work supported by the National Science Foundation under Grant No. 1537626. Their support is gratefully acknowledged. Any opinions, findings, and conclusions or recommendations expressed in this material are those of the authors and do not necessarily reflect the views of the sponsor.

References

[1] ASCE 7-16, Minimum Design Loads and Associated Criteria for Buildings and Other Structure, ASCE/SEI 7-16, 2017.

[2] Kareem, A., Kijewski, T., & Tamura, Y., "Mitigation of motions of tall buildings with specific examples of recent applications.," *Wind and structures,* pp. 201-251, 1999.

[3] Tamura Y, Kareem A., Advanced structural wind engineering, New York: Springer, 2013.

[4] Bernardini, E., Spence, S. M., Wei, D., & Kareem, A., "Aerodynamic shape optimization of civil structures: A CFD-enabled Kriging-based approach," *Journal of Wind Engineering and Industrial Aerodynamics,* pp. 144, 154-164, 2015.

[5] Mooneghi, M. A., & Kargarmoakhar, R., "Aerodynamic mitigation and shape optimization of buildings," Journal of building engineering, Vols. 6, 225-235, 2016.

[6] Spence, S. M., & Gioffrè, M., "Large scale reliability-based design optimization of wind excited tall buildings," Probabilistic Engineering Mechanics, pp. 28, 206-215, 2012.

[7] Gholizadeh, S., & Fattahi, F. (2014). Design optimization of tall steel buildings by a modified particle swarm algorithm. . The Structural Design of Tall and Special Buildings, 23(4), 285-301.

[8] Huang, M. F., Li, Q., Chan, C. M., Lou, W. J., Kwok, K. C., & Li, G. (2015). Performance-based design optimization of tall concrete framed structures subject to wind excitations. Journal of Wind Engineering and Industrial Aerodynamics, 139, 70-81.

[9] Tse, K. T., Kwok, K. C., & Tamura, Y., "Performance and cost evaluation of a smart tuned mass damper for suppressing wind-induced lateral-torsional motion of tall structures," Journal of Structural Engineering, pp. 138(4), 514-525, 2012.

[10] Aly, A. M., Zasso, A., & Resta, F, "On the dynamics of a very slender building under winds: response reduction using MR dampers with lever mechanism," The structural design of tall and special buildings, pp. 20(5), 539-551, 2011.

[11] Cao, L., Laflamme, S., Hong, J., & Dodson, J., "Input space dependent controller for civil structures exposed to multi-hazard excitations," Engineering Structures, pp. 166, 286-301, 2018.

[12] Laflamme, S., Taylor, D., Abdellaoui Maane, M., & Connor, J. J., "Modified friction device for control of large-scale systems," Structural control and health monitoring, pp. 19(4), 548-564, 2012.

[13] Venanzi, I., & Materazzi, A. L., "Multi-objective optimization of wind-excited structures," Engineering Structures, pp. 29(6), 983-990, 2007.

[14] Aly, A. M., "Proposed robust tuned mass damper for response mitigation in buildings exposed to multidirectional wind," The structural design of tall and special Buildings, pp. 23(9), 664-691, 2014.

[15] Chan, C. M., Huang, M. F., & Kwok, K. C., "Stiffness optimization for wind-induced dynamic serviceability design of tall buildings," Journal of structural engineering, pp. 135(8), 985-997, 2009.

[16] Li, Q. S., Zou, X. K., Wu, J. R., & Wang, Q., "Integrated wind-induced response analysis and design optimization of tall steel buildings using Micro-GA," The Structural Design of Tall and Special Buildings, pp. 20, no. 8 (2011): 951-971, 2011.

[17] Venanzi, I., Ubertini, F., & Materazzi, A. L., "Optimal design of an array of active tuned mass dampers for wind-exposed high-rise buildings," Structural Control and Health Monitoring, pp. 20(6), 903-917, 2013.

[18] Micheli, L., Alipour, A., Laflamme, S., & Sarkar, P, "Performance-based design with life-cycle cost assessment for damping systems integrated in wind excited tall buildings," Engineering Structures, pp. 195, 438-451, 2019.

[19] Echard, B., Gayton, N., Lemaire, M., & Relun, N., "A combined importance sampling and kriging reliability method for small failure probabilities with time-demanding numerical," Reliability Engineering & System Safety, pp. 111, 232-240, 2013.

[20] Bichon, B. J., McFarland, J. M., & Mahadevan, S., "Efficient surrogate models for reliability analysis of systems with multiple failure modes," Reliability Engineering & System Safety, pp. 96(10), 1386-1395, 2011.

[21] Ferrario, E., Pedroni, N., Zio, E., & Lopez-Caballero, F., "Bootstrapped Artificial Neural Networks for the seismic analysis of structural systems," Structural Safety, pp. 67, 70-84, 2017.

[22] Abdallah, I., Lataniotis, C., & Sudret, B., "Hierarchical Kriging for multi-fidelity aero-servo-elastic simulators-Application to extreme loads on wind turbines," Probabilistic Engineering Mechanics, pp. 55, 67-77, 2019.

[23] Gholizadeh, S., & Aligholizadeh, V., "Reliability-based optimum seismic design of RC frames by a metamodel and metaheuristics," The Structural Design of Tall and Special Buildings, pp. 28(1), e1552., 2019.

[24] Forrester, A. I., & Keane, A. J., "Recent advances in surrogate-based optimization," Progress in aerospace sciences, pp. 45(1-3), 50-79, 2009.

[25] Blatman, G., & Sudret, B, "An adaptive algorithm to build up sparse polynomial chaos expansions for stochastic finite element analysis," Probabilistic Engineering Mechanics, pp. 25(2), 183-197, 2010.

[26] Moustapha, M., Bourinet, J. M., Guillaume, B., & Sudret, B., "Comparative Study of Kriging and Support Vector Regression for Structural Engineering Applications," ASCE-ASME Journal of Risk and Uncertainty in Engineering Systems, Part A: Civil Engineering, pp. 4(2), 04018005, 2018.

[27] Sudret, B., & Mai, C. V., "Computing seismic fragility curves using polynomial chaos expansions," in 11th International Conference on Structural Safety and Reliability (ICOSSAR), Zürich, 2013.

[28] Gidaris, I., Taflanidis, A. A., & Mavroeidis, G. P., "Kriging metamodeling in seismic risk assessment based on stochastic ground motion models," Earthquake Engineering & Structural Dynamics, pp. 44(14), 2377-2399, 2015.

[29] Gidaris, I., Taflanidis, A. A., Lopez-Garcia, D., & Mavroeidis, G. P., "Multi-objective risk-informed design of floor isolation systems," Earthquake Engineering & Structural Dynamics, pp. 45(8), 1293-1313, 2016.

[30] Micheli, L., Alipour, A., & Laflamme, S., "Data-driven risk-based assessment of wind-excited tall buildings using surrogate models," in Structures Congress 2019: Blast, Impact Loading, and Research and Education, 2019.

[31] Micheli, L. , Hong, J., Laflamme, S. & Alipour, A., "Surrogate Models for High Performance Control Systems in Wind-excited Tall Building," Applied Soft Computing, p. 106133, 2020.

[32] Federal Emergency Management Agency (FEMA-P-58), "Seismic performance assessment of buildings, Volume 1 - Methodology," Washington, DC: FEMA Publication P-58-1, 2012.

[33] McNamara, R. J., Huang, C. D., & Wan, V., "Viscous-damper with motion amplification device for high rise building applications," Advanced Technology in Structural Engineering, pp. pp. 1-10, 2000.

[34] Mcnamara, R. J., & Taylor, D. P., "Fluid viscous dampers for high-rise buildings," The structural design of tall and special buildings, pp. 145-154, 2003.

[35] Connor, J., & Laflamme, S., "Structural motion engineering," Springer, 2014.

[36] Cao, L., Laflamme, S., Taylor, D., & Ricles, J., "Simulations of a variable friction device for multihazard mitigation," Journal of Structural Engineering, pp. 142, no. 12 (2016): H4016001, 2016.

[37] Simiu, E., & Scanlan, R. H., "Wind effects on structures: fundamentals and applications to design," 1996.

[38] Deodatis, G., "Simulation of ergodic multivariate stochastic processes," Journal of engineering mechanics, pp. 778-787, 1996.

[39] Lamb, S., Kwok, K. C., & Walton, D., "A longitudinal field study of the effects of wind-induced building motion on occupant wellbeing and work performance," Journal of wind engineering and industrial aerodynamics, 2014.

[40] Lamb, S., & Kwok, K. C. S., "Sopite syndrome in wind-excited buildings: productivity and wellbeing impacts.," Building Research & Information, pp. 1-12, 2016.

[41] Cui, W., & Caracoglia, L., "Simulation and analysis of intervention costs due to wind-induced damage on tall buildings," Engineering Structures, pp. 183-197, 2015.

[42] Ierimonti, L., Venanzi, I., & Caracoglia, L., "Life-cycle damage-based cost analysis of tall buildings equipped with tuned mass dampers," Journal of Wind Engineering and Industrial Aerodynamics, pp. 176, 54-64, 2018.

[43] Ierimonti, L., Caracoglia, L., Venanzi, I., & Materazzi, A. L., "Investigation on life-cycle damage cost of wind-excited tall buildings considering directionality effects," Journal of Wind Engineering and Industrial Aerodynamics, pp. 171, 207-218, 2017.

[44] Taflanidis, A. A., & Beck, J. L., "Life-cycle Cost Optimal Design of Passive Dissipative Devices for Seismic Risk Mitigation," Proceedings of the 10th International Conference on Structural Safety and Reliability, pp. (pp. 467-467). CRC Press, 2009.

[45] "Taylor Devices," 2019. [Online].

[46] Forrester, A., Sobester, A., & Keane, A, "Engineering design via surrogate modelling: a practical guide," *John Wiley & Sons.,* 2008.

[47] Higham, N. J., "Computing a nearest symmetric positive semidefinite matrix," Linear algebra and its applications, 1988.

[48] Jafari, M., & Alipour, A. "Methodologies to mitigate wind-induced vibration of tall buildings: A state-of-the-art review," *Journal of Building Engineering*, 101582, 2020.

[49] Micheli, L., Alipour, A., & Laflamme, S. "Multiple-Surrogate Models for Probabilistic Performance Assessment of Wind-Excited Tall Buildings under Uncertainties," ASCE-ASME Journal of Risk and Uncertainty in Engineering Systems, Part A: Civil Engineering, 6(4), 04020042, 2020.

[50] Micheli, L., Cao, L., Laflamme, S., & Alipour, A. "Life-cycle cost evaluation strategy for high-performance control systems under uncertainties," *Journal of Engineering Mechanics*, *146*(2), 04019134, 2020.

[51] Micheli, L., Alipour, A., & Laflamme, S. "Performance-based design for wind-excited tall buildings equipped with high performance control systems," In *Structures Congress 2018: Buildings and Disaster Management* (pp. 179-191). Reston, VA: American Society of Civil Engineers, 2018, April.

[52] Micheli, L., Cao, L., Gong, Y., Cancelli, A., Laflamme, S., & Alipour, A. "Probabilistic performance-based design for high performance control systems," In *Active and Passive Smart Structures and Integrated Systems 2017* (Vol. 10164, p. 101642I). International Society for Optics and Photonics, 2017, April.

[53] Micheli, L., & Laflamme, S. "Kriging-based design for robust high-performance control systems," *ASCE-ASME Journal of Risk and Uncertainty in Engineering Systems, Part A: Civil Engineering*, *6*(4), 04020037, 2020.